SUPPLEMENTAL MATERIAL

Rujano et al., https://doi.org/10.1084/jem.20170453

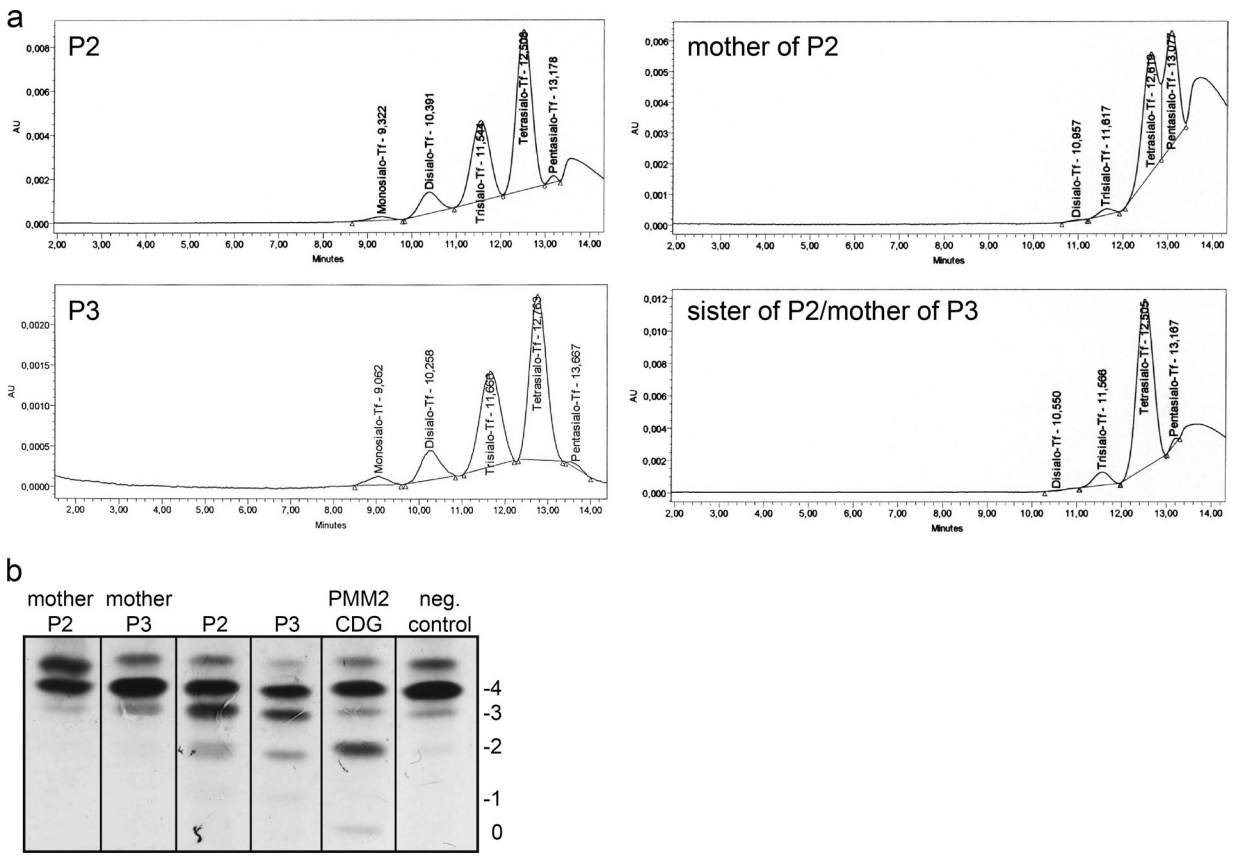

Figure S1. **Glycosylation diagnostics for patient P2 and P3 with missense mutations.** (a) HPLC of serum transferrin in a sample from P2 revealed elevated mono- (1.7%), di- (10.0%), and trisialo-transferrin (34.9%), whereas tetrasialo-transferrin was found to be reduced (53.3%). P3 shows a similar dysglycosylation pattern with elevated mono- (3.14%), di- (10.27%), and trisialo-transferrin (35.41%) as well as diminished tetrasialo-transferrin (50.28%). The samples of both unaffected relatives show a grossly normal transferrin glycosylation with a slight increase of tri- and pentasialo-transferrin, respectively (b). HPLC reference ranges are as followed: asialo-transferrin 0%, monosialo-transferrin 0%, disialo-transferrin 0.38–1.82%, trisialo-transferrin 1.16–6.36%, tetrasialo-transferrin 85.7–94.0%, and pentasialo-transferrin 2.6–10.2%. (b) Isoelectric focusing of serum transferrin samples from family F2. Analysis of samples from P2 and P3 revealed a type II congenital disorder of glycosylation (CDG) pattern with increased tri- (-3), di- (-2), and monosialo-transferrin (-1), whereas tetrasialo-transferrin is diminished. Serum samples of P2's mother (mother P2) and sister (sister P2/mother P3) show grossly normal transferrin glycosylation except for a slightly increase in trisialo-transferrin in the sister's sample as well as an increase of pentasialo-transferrin in the mother's sample. AU, arbitrary units; neg., negative.

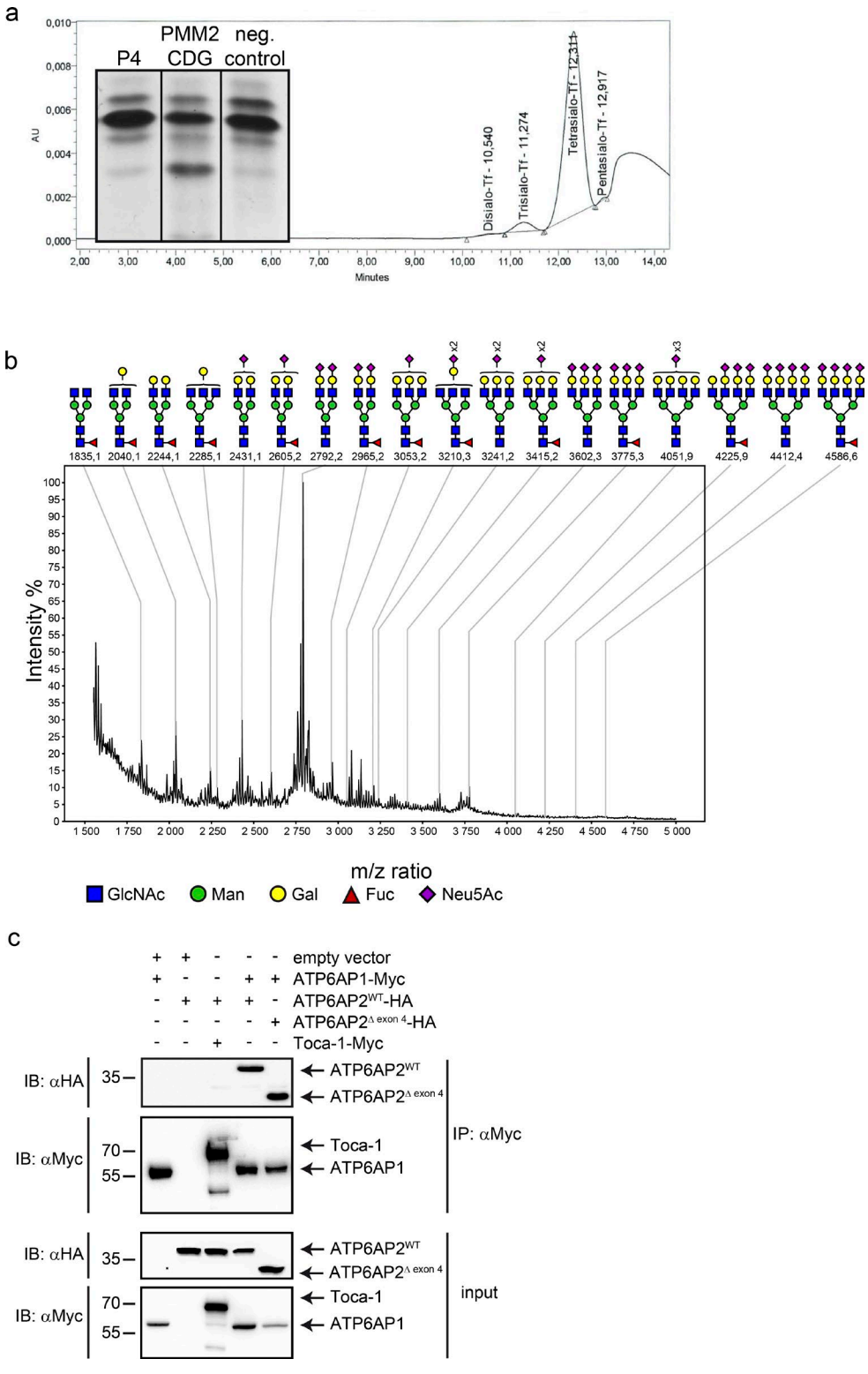

Figure S2. **Characteristics of a patient with exon-skipping mutation (P4).** (a) Isoelectric focusing (IEF) and HPLC of serum transferrin samples from P4 revealed a normal glycosylation pattern. (b) Representative MALDI-TOF MS spectra of permethylated N-glycans derived from the serum of patient P4 (Korvatska et al., 2013). P4 N-glycoproteins show only a very mild undersialylation compared with the L98S patient. (c) CoIP in HEK293T cells using the indicated constructs. Proteins were immunoprecipitated with anti-Myc antibody and cell lysates were subjected to immunoblotting with anti-HA and anti-Myc antibodies. Data in (c) are representative of two independent experiments. AU, arbitrary units; neg., negative. Molecular mass is indicated in kilodaltons.

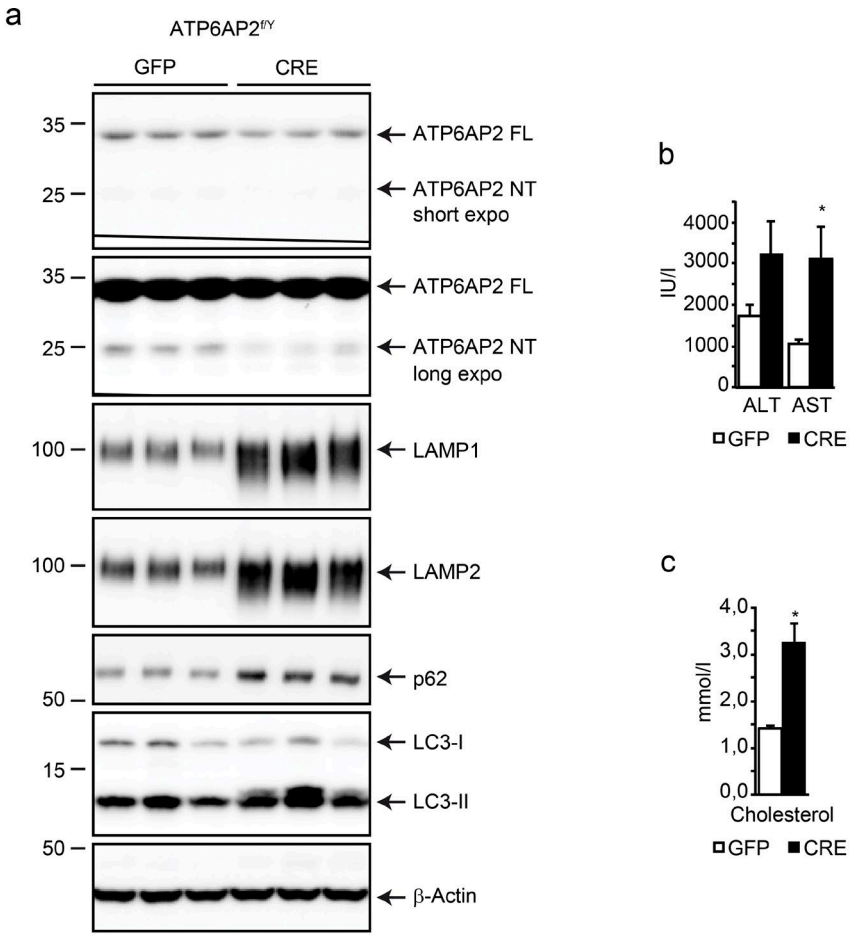

d

mass m/z																	
1578.7		1660.7		1834.7		2039.7		2256.6		2460.6		2606.8		2634.5		2851	
GFP	CRE	GFP	CRE	GFP	CRE	GFP	CRE	GFP	CRE	GFP	CRE	GFP	CRE	GFP	CRE	GFP	CRE
3,30	0,00	0	30,9	10,35	22,7	11,8	24,9	7	40,8	14,7	32,2	16,9	28	13,3	25,6	100	100
3,50	7,50	0	0	9,12	18,9	12,6	25	6,9	12,3	14,9	22,7	18,3	0	15,1	19,3	100	100
0,00	24,4	0	53,9	18,2	42	22,7	43,1	8,7	75,5	18,3	36,5	0	0	16,4	21,3	100	100
6,60	0,00	0	25,7	10,2	21	15,4	21,5	9,2	33	15,7	28,8	0	0	13,6	17,8	100	100
6,80	20,1	0	54,4	11,6	24,6	15,9	30,2	10,9	58	20,4	28,6	0	0	13,4	16,3	100	100
0,00		0		0		5,2		4,9		9,9		0		9,9		100	
7,90		0		17,2		18,7		12,3		22,1		13		13,3		100	

Figure S3. **Characterization of ATP6AP2 conditional knockout (cKO) mice.** (a) Immunoblot analysis of liver tissue extracts with indicated antibodies. Male mice carrying a floxed allele of the X-linked *ATP6AP2* mice were transduced with adeno-GFP or adeno-CRE viral vectors and tissue collected 10 d after injection in a random-fed state. The protein bands on the respective immunoblot panels are indicated by arrows. β-Actin served as a loading control. Molecular mass is indicated in kilodaltons. (b) Plasmatic ALT and AST. (c) Total serum cholesterol levels. Samples are derived from random fed male mice treated as in a. Data are mean ± SEM of six to eight independent experiments. Significance was determined by a two-tailed unpaired Student's *t* test. *, $P < 0.05$. (d) Permethylation and MALDI-TOF MS analysis of *N*-glycans from controls (GFP, $n = 7$) and *ATP6AP2* cKO mice (CRE, $n = 5$) were performed as described in Materials and methods. Relative intensities of significantly altered *N*-glycan structures (mass m/z: 1660, 1835, 2040, 2256, 2460) were determined taking into account peak 2851(m/z) as 100%. Red boxes indicate underglycosylated side chains with the corresponding values in gray for adeno-CRE.

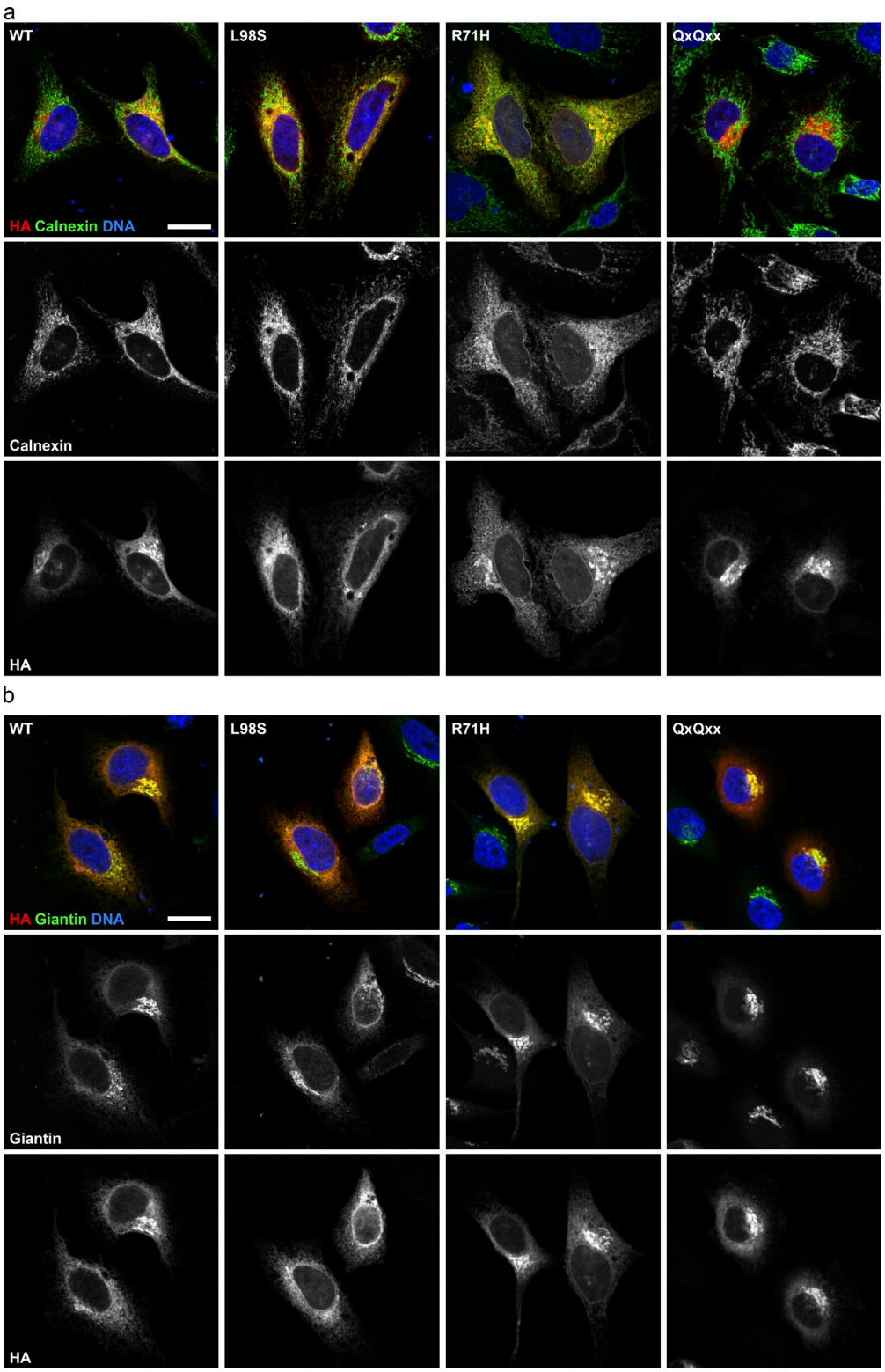

Figure S4. **Localization studies of ATP6AP2 constructs in HeLa cells.** (a) Colocalization studies of ATP6AP2^{WT}, ATP6AP2^{L98S}, ATP6AP2^{R71H}, and ATP6AP2^{QxQxx} in overexpression. ATP6AP2 constructs are stained with anti-HA antibody (red), ER with anti-Calnexin (green), and DNA stained with Hoechst (blue). (b) Colocalization studies with ATP6AP2 constructs stained with anti-HA antibody (red), Golgi with anti-Giantin (green), and DNA stained with Hoechst (blue). Images in a and b are representative of two independent experiments. Bars, 20 µm.

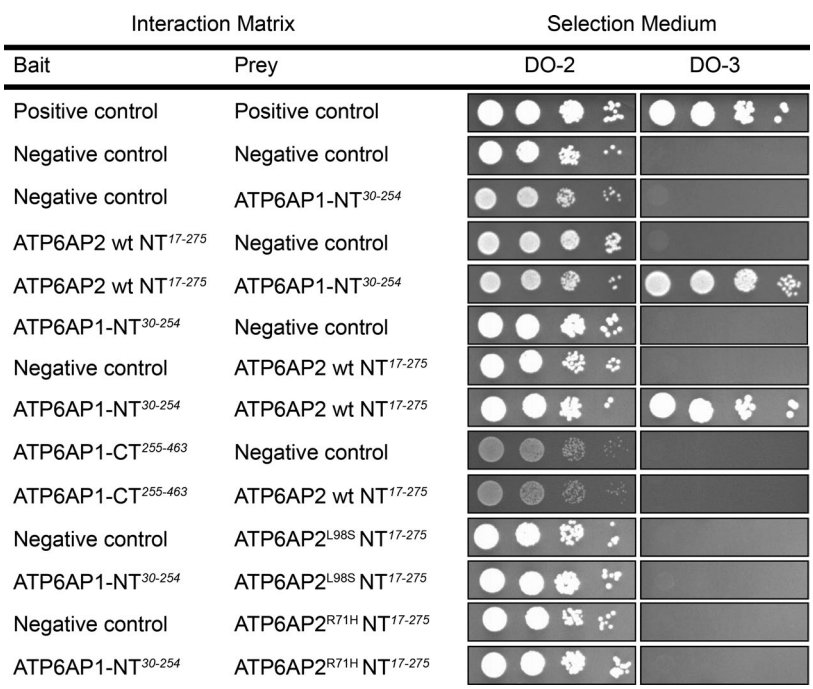

Figure S5. **The interaction of ATP6AP2 with ATP6AP1 is lost in the missense mutants.** Direct 1-by-1 Y2H assay for protein–protein interactions. Different fragments of mouse ATP6AP1, ATP6AP2^{WT}, ATP6AP2^{L98S}, and ATP6AP2^{R71H} proteins were expressed in yeast as bait and prey as indicated. Cells were grown in DO-2 selective medium without tryptophan and leucine or in DO-3 selective medium without tryptophan, leucine, and histidine. Growth in DO-3 medium indicates a positive protein–protein interaction.

Table S1. ***Drosophila* genotypes used in this study**

Genotype	Figure
w^{1118}	Fig. 6, a–e and g
	Fig. 7, a–d
	Fig. 9, e and g
w; ATP6AP2>*ATP6AP2*^{L98S}; FRT82B, *ATP6AP2*$^{\Delta 1}$	Fig. 6, a–e and g
	Fig. 7, a–d
	Fig. 9, e and g
w; ATP6AP2>*ATP6AP2*$^{WT\text{-}myc}$; FRT82B, *ATP6AP2*$^{\Delta 1}$	Fig. 6, c and d
	Fig. 7 d
	Fig. 9 e
w; ATP6AP2>*ATP6AP2*$^{\Delta KKxx}$; FRT82B, *ATP6AP2*$^{\Delta 1}$	Fig. 6, a–d
	Fig. 7 d
	Fig. 9 e
w; ATP6AP2>*ATP6AP2*^{AxxA}; FRT82B, *ATP6AP2*$^{\Delta 1}$	Fig. 6, a–d
	Fig. 7 d
	Fig. 9 e
w; ATP6AP2>*ATP6AP2*^{WT}; FRT82B, *ATP6AP2*$^{\Delta 1}$	Fig. 6, a, b, and e
hs-Flp; FRT42D, ATP6AP2>*ATP6AP2*^{WT}, ubi-mRFP.nls/FRT42D, ATP6AP2>*ATP6AP2*^{L98S}; *ATP6AP2*$^{\Delta 1}$	Fig. 7 e
	Fig. 9, a, d, and f
hs-Flp; tub-FRT-Gal80-FRT-Gal4, UAS–mCD8–mRFP/+; UAS-ATP6AP2 RNAi (Vienna, GD5830)/+	Fig. 7, f and g
hs-Flp; tub-FRT-Gal80-FRT-Gal4, UAS–mCD8–mRFP/+; UAS-ATP6V1C1 RNAi (Vienna, KK101527)/+	Fig. 7, f and g
hs-Flp; tub-FRT-Gal80-FRT-Gal4, UAS–mCD8–mRFP/+; UAS-ATP6AP1 RNAi (Vienna, GD48017)/+	Fig. 7, f and g
hs-Flp; Tub>GFP-Lamp/+; Tub-FRT-Gal80-FRT-Gal4, UAS-mCD8-RFP/UAS-ATP6AP2 RNAi (Vienna, GD5830)	Fig. 9 b
hs-Flp; UAS-Dcr2; R4-mCherry-Atg8, Actin-FRT-CD2-FRT-Gal4, UAS-GFPnls/UAS-ATP6AP2 RNAi (Vienna, GD5830)	Fig. 9 c
ptc-GAL4; UAS-*ATP6AP2*^{WT}/+	Fig. 5 c
ptc-GAL4; UAS-*ATP6AP2*^{L98S}/+	Fig. 5 c
ap-GAL4; UAS-ATP6AP2 RNAi (Vienna, GD5830)/+	Fig. 9 h

REFERENCE

Korvatska, O., N.S. Strand, J.D. Berndt, T. Strovas, D.H. Chen, J.B. Leverenz, K. Kiianitsa, I.F. Mata, E. Karakoc, J.L. Greenup, et al. 2013. Altered splicing of ATP6AP2 causes X-linked parkinsonism with spasticity (XPDS). *Hum. Mol. Genet.* 22:3259–3268. https://doi.org/10.1093/hmg/ddt180